Journal of Hazardous Materials 188 (2011) 105–109

Contents lists available at ScienceDirect

Journal of Hazardous Materials

journal homepage: www.elsevier.com/locate/jhazmat

Catalytic reduction of NO_x with NH_3 over different-shaped MnO_2 at low temperature

Wei Tian, Hangsheng Yang*, Xiaoyu Fan, Xiaobin Zhang

State Key Laboratory of Silicon Materials, Department of Materials Science and Engineering, Zhejiang University, Zheda Road 38, Hangzhou 310027, China

ARTICLE INFO

Article history:
Received 10 September 2010
Received in revised form 17 January 2011
Accepted 18 January 2011
Available online 26 January 2011

Keywords:
SCR
MnO_2
Hydrothermal method
NO_x
Apparent activation energy

ABSTRACT

MnO_2 nanotubes, nanorods, and nanoparticles were prepared using a hydrothermal method, after which the different activities for selective catalytic reduction (SCR) of nitrogen oxides (NO_x) were compared. MnO_2 nanorods performed the highest activity for reduction of NO_x under a gas hourly space velocity of 36,000 h^{-1} with conversion efficiencies of above 90% between 250 and 300 °C; it also had the highest removal efficiency of 98.2% at 300 °C. From the analysis of X-ray diffraction, scanning electron microscopy, X-ray photoelectron spectroscopy, temperature-programmed desorption, and temperature-programmed reduction, we can ascribe the high activity of MnO_2 nanorods to low crystallinity, more lattice oxygen, high reducibility, and a large number of strong acid sites. The apparent activation energy of the SCR reaction on the surface of nanorods was calculated to be 20.9 kJ/mol, which favored the reaction better than the other catalysts.

1. Introduction

Nitrogen oxides (NO_x) are major environmental pollutants and have detrimental effects on human health. NO is the main component of NO_x, which is generated through the combustion processes (stationary and mobile) [1,2]. NO_x contributes to acid rain, formation of photochemical smog and ozone layer depletion, which has attracted much attention all over the world. Due to the increasing threat of NO_x to our survival, many approaches have been developed to reduce its emission, among which selective catalytic reduction technique (SCR) is proven to be an effective way compared with other NO_x abatement technologies, such as nonselective catalytic reduction technique, storage, and thermal decomposition [3,4].

Many catalysts have been reported to be active in NH_3-SCR technology [5,6]. Commercially available catalysts are mainly based on V_2O_5/TiO_2 [7]. Due to the fact that these catalysts only exhibit high NO_x conversions in the temperature range of 300–400 °C, SCR systems are normally installed prior to particle removal facility [8]. However, high concentrations of particles and other contaminants are deleterious for the catalyst; thus, locating the SCR system after the particle removal facility, where the flue gas temperature is usually below 300 °C, is highly desired. Therefore, there is a great interest in the development of SCR catalysts that are active at low temperatures.

Many catalysts consisting of various transition metal oxides (V, Cr, Mn, Fe, Co, Ni, and Cu oxides) on different commercial supports, such as silica and alumina, have been studied. Among them, MnO_x-based catalysts have attracted much attention because of their high activity for SCR reaction and for various other reactions, such as oxidative coupling of methane [9], CO and CH_4 oxidation [9,10], oxidative dehydrogenation [11,12], and total oxidation of VOCs [13,14]. For example, MnO_x/Al_2O_3 [15], MnO_x/NaY [16], MnO_x/USY [17], MnO_x/TiO_2 [10,11,18], and unsupported MnO_x [19] have been shown to perform high catalytic activities for NO_x removal. In this report, unsupported MnO_2 catalysts with different shapes have been prepared, after which their activities for NO_x removal are studied. The results showed that among them, MnO_2 nanorods exhibited excellent catalytic activity in the temperature range of 100–300 °C.

2. Experiments

2.1. Catalyst preparation

Catalysts were prepared using a hydrothermal approach [20,21]. In a typical experimental procedure for MnO_2 nanotube preparation, 2 mmol $KMnO_4$ and 8 mmol HCl were added to 45 ml deionized water to form the precursor solution. This was then transferred into a Teflon-lined stainless steel autoclave with a capacity of 65 ml. The autoclave was sealed and hydrothermally treated at 140 °C for 12 h. Once the autoclave was cooled down to room temperature naturally, the black precipitates were collected by centrifugation and washed several times using deionized

* Corresponding author. Tel.: +86 571 87951404; fax: +86 571 87951404.
E-mail address: hsyang@zju.edu.cn (H. Yang).

0304-3894/$ – see front matter © 2011 Elsevier B.V. All rights reserved.
doi:10.1016/j.jhazmat.2011.01.078

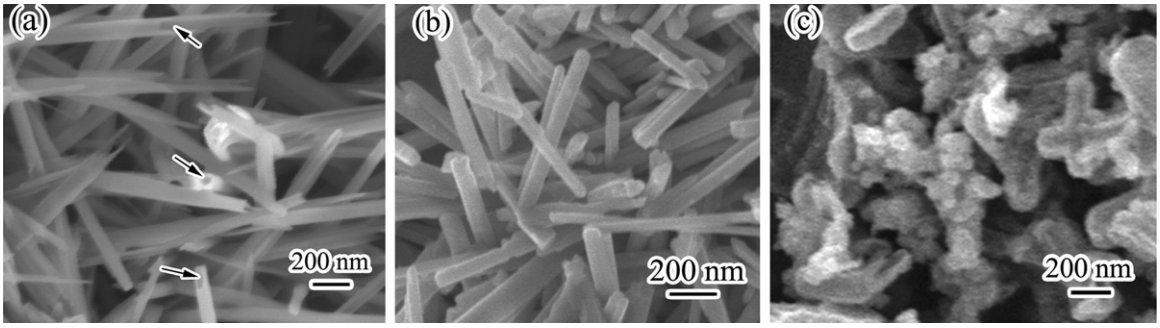

Fig. 1. SEM images of the catalysts. (a) MnO_2 nanotubes; (b) MnO_2 nanorods; and (c) MnO_2 nanoparticles.

water to remove possible impurities or excess ions. The as-prepared sample was then dried in air overnight. To prepare the MnO_2 nanorods, 3 mmol $Mn(CH_3COO)_2$ was added into the $KMnO_4$ + HCl aqueous solution and heated at 180 °C for 12 h. To prepare the MnO_2 nanoparticles, the heat temperature was changed to 220 °C, and additive of NaF was added in the nanorod synthesis procedure.

2.2. Catalyst characterization

X-ray diffraction (XRD) pattern was recorded on a Philips XD-98 X-ray diffractometer using Cu Kα radiation (λ = 0.15406 nm). The morphology was observed by scanning electron microscopy (SEM) (JEOL S-4800). X-ray photoelectron spectroscopy (XPS) data were obtained using Kratos Axis Ultra-DLD, in which C 1s = 284.8 eV was used as internal reference for the data processing of the XPS. The temperature-programmed reduction (H_2-TPR) experiment was carried out for every 50 mg of catalyst from 100 to 1000 °C with a 1690 Gas Chromatograph. Prior to the analysis, the catalysts were pretreated at 300 °C for 0.5 h in air. The TPR runs were carried out with a linear heating rate (10 °C/min) in a mixed flow of 5% H_2 in argon with a flow rate of 40 ml/min. An NH_3-temperature-programmed desorption (NH_3-TPD) experiment was performed to determine the acidity of catalysts. Here, 50 mg of every catalyst was loaded in the reactor and pretreated in a He stream (30 ml/min) at 550 °C for 1 h, and then cooled to 100 °C in the same stream. The pretreated sample was then exposed to NH_3 (4%) at a flow rate of 20 ml/min for 3 h. The physisorbed NH_3 was removed by flushing the catalysts with N_2 at a flow rate of 30 ml/min for 1 h before starting the TPD experiment. Experimental runs were recorded by heating the samples in N_2 (30 ml/min) from 100 to 700 °C at a heating rate of 10 °C/min. Both the H_2-TPR and NH_3-TPD experiments were analyzed in an online gas chromatographer using a TCD detector.

2.3. Catalytic experiments

Catalytic activity tests were carried out in a flow reactor of a fixed-bed tank. All catalysts were grounded and mixed with 25 wt% organoclay and then pasted on ten 3 cm × 10 cm aluminum plates. The prepared catalytic plates were inserted into the grooves of the reactor; the distance between plates was 5–6 mm. An NO–NO_2–NO_x analyzer (Testo AG–testo 350) was used to measure the inlet and outlet concentrations of NO and NO_2. The catalyst temperature was measured through a thermocouple projecting into the center of the reactor. The air flowing through silica gel to remove the water before introduction to the reactor was mixed in as the source of O_2 and N_2. The premixed gases (0.9% NO/Ar, 1% NH_3/Ar) were prepared to formulate the flue gas in the experiment. The reactant gas feed, consisting of NO_x (550 ppm), O_2 (6 vol%), NH_3 (550 ppm), and N_2 as balanced gas, was introduced to the reactor at a total flow rate of 500 ml/min, corresponding to a GHSV of 36,000 h^{-1}. Water vapor (2.5 vol%) was generated by passing N_2 through a gas-wash bottle containing deionized water. The reacting gases were mixed and preheated at 100 °C before the reactor entrance. The activity tests were performed from 100 to 300 °C with a step of 25 °C.

3. Results and discussion

3.1. SEM and XRD analysis

Fig. 1 shows the SEM image of the as-prepared MnO_2 nanostructures. High-purity nanotubes were successfully prepared; the diameter of the nanotubes ranged from 30 to 100 nm, and a length of more than 1 μm (Fig. 1a). The MnO_2 nanorods also showed high morphological purity with a diameter between 100 and 200 nm, and a length between 500 nm and 1 μm (Fig. 1b). Meanwhile, Fig. 1c shows the irregular particle-like morphology of the β-MnO_2. As shown in Fig. 2, all the diffraction peaks of the nanotubes can be exclusively indexed as the tetragonal α-MnO_2 structure (JCPDS 44-0141). For the nanorods, in addition to the peaks of α-MnO_2, several small peaks assigned to the β-MnO_2 (JCPDS 65-2821) were also observed, indicating that the MnO_2 nanorods here mainly existed in the α phase. For the MnO_2 nanoparticles, all peaks corresponded to the β-MnO_2 (JCPDS 65-2821). From the intensity of the peaks and full width at half maximum, the MnO_2 nanotubes and nanorods were of low crystallinity compared with the nanoparticles.

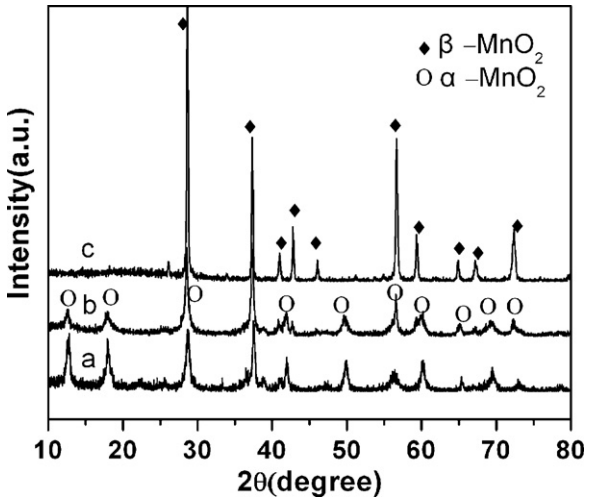

Fig. 2. XRD patterns of the catalysts. (a) MnO_2 nanotubes; (b) MnO_2 nanorods; and (c) MnO_2 nanoparticles.

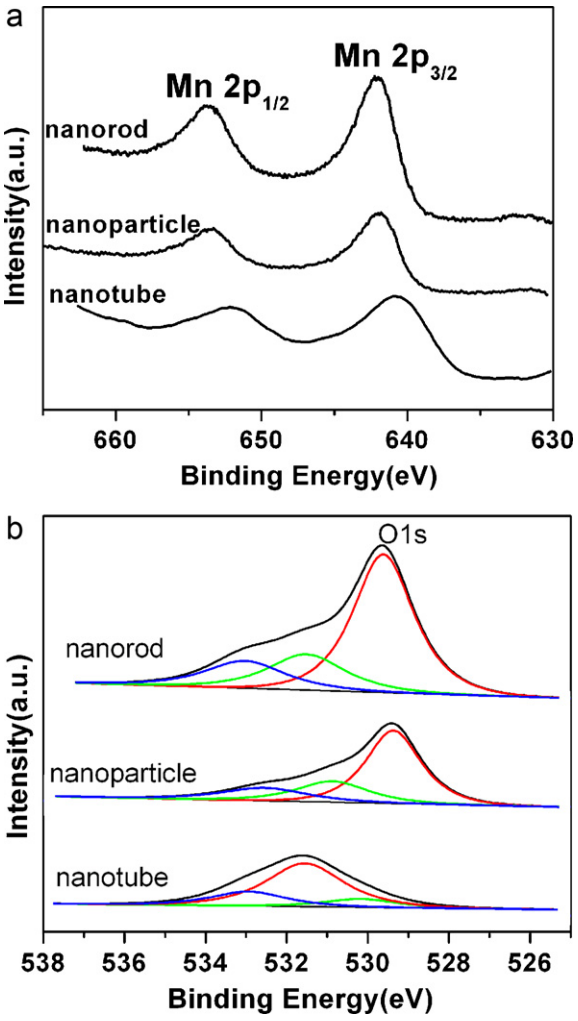

Fig. 3. XPS spectra of MnO_2 nanotubes, nanorods, and nanoparticles. (a) Mn 2p spectra; and (b) O 1s spectra.

3.2. XPS analysis

Fig. 3 shows the XPS spectra of the catalysts. The Mn 2p core level spectra in Fig. 3a illustrate the binding energies for Mn $2p^{3/2}$ and Mn $2p^{1/2}$, where a binding energy of 642 ± 0.2 eV suggests the existence of only Mn^{4+} of MnO_2, and an energy separation of 11.5 eV is observed between the Mn $2p^{3/2}$ and Mn $2p^{1/2}$ states. All these features are consistent with the values reported in literature [22,23]. The O 1s binding energy 529.2 ± 0.4 eV in Fig. 3b can be ascribed to the lattice oxygen ions (O_L) bound to Mn [24]. The peaks at 530–533 eV can be attributed to the surface oxygen and surface hydroxyl groups (O_S) bound to Mn [25,26]. The ratios of $O_L/(O_L + O_S)$ on the surface of MnO_2 nanorods, nanoparticles, and nanotubes were approximately 63.8%, 60.8% and 11.7%, respectively.

3.3. TPR and TPD analyses

Fig. 4 shows the TPR spectra of three samples. For MnO_2 nanotubes, the TPR profile shows three overlapped peaks ranging from 350 to 600 °C that correspond to the reduction of MnO_2 to Mn_2O_3, Mn_2O_3 to Mn_3O_4 and Mn_3O_4 to MnO, respectively [27,28]. The TPR curves of the nanorods showed two overlapped peaks, corresponding to the reduction of MnO_2 to Mn_3O_4 and Mn_3O_4 to MnO, respectively. This observation is in accordance with the previous reports stating that the reduction of MnO_2 with low crystallinity

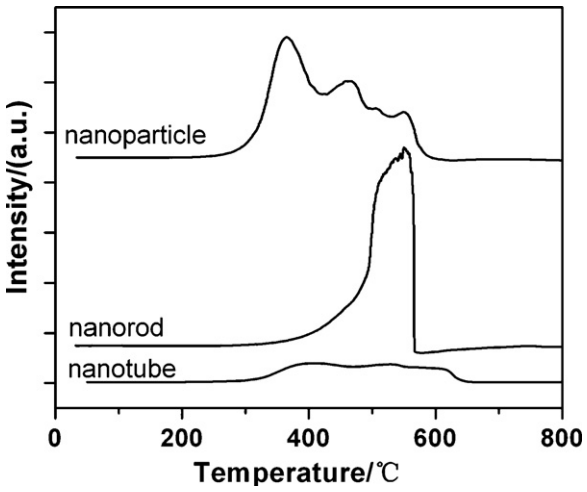

Fig. 4. TPR patterns of MnO_2 nanotubes, nanorods, and nanoparticles.

takes place through a distinct two-step process [29]: the first step involves the reduction of MnO_2 to Mn_3O_4, and the second step represents the reduction of Mn_3O_4 to MnO. For the nanoparticles, the curve contains three overlapped peaks corresponding to the reduction of MnO_2 to Mn_2O_3, Mn_2O_3 to Mn_3O_4 and Mn_3O_4 to MnO, respectively [27,28]. The H_2 consumption levels for MnO_2 nanorod, nanoparticle, and nanotube calculated from Fig. 4 were approximately 11.39, 11.20 and 2.93 mmol/g, respectively.

The NH_3-TPD patterns of these catalysts are shown in Fig. 5. The NH_3-TPD spectra of the MnO_2 nanotubes contain only a single main peak ranging from 400 to 550 °C, which signifies a distribution of weak acid sites. The peak could be assigned to the successive desorption of ammonia physisorbed to weak acid sites and likely linked to Bronsted acid sites (250–440 °C) [30]. For the MnO_2 nanorods, the NH_3-TPD curve showed two peaks – the first one centered at about 760 °C and the second one centered at about 830 °C – that can be attributed to NH_3 desorbed from Lewis acid sites [31]. The shape of the NH_3-TPD pattern obtained from the nanoparticles was very similar to that of the nanorods; in addition, their desorption temperatures all shifted to a high temperature, suggesting the presence of strong acid sites on the surface. The ratios of desorption amounts of NH_3 for MnO_2 nanorods, nanoparticles, and nanotubes were

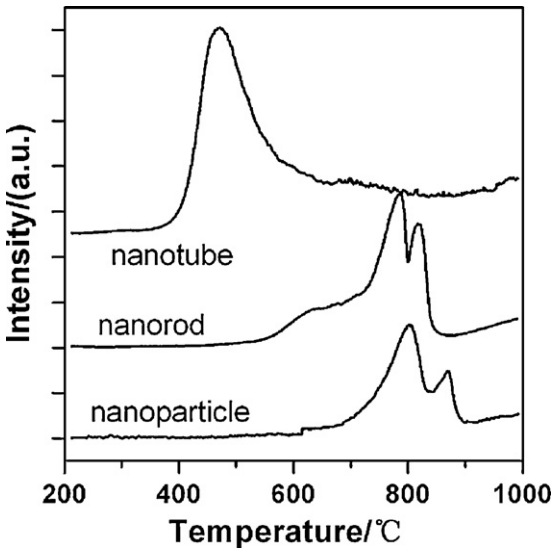

Fig. 5. TPD patterns of MnO_2 nanotubes, nanorods, and nanoparticles.

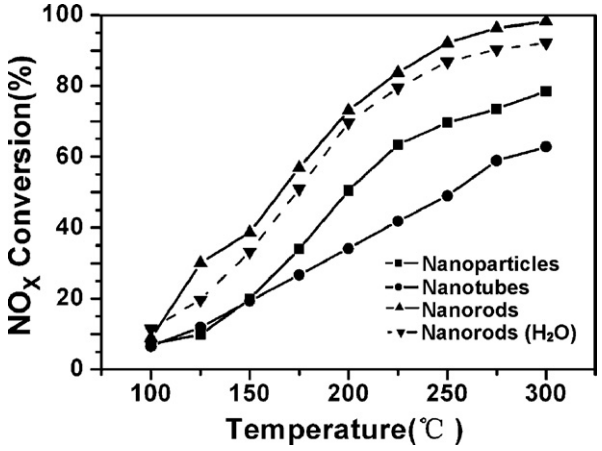

Fig. 6. NO_x conversion of MnO_2 nanotubes, nanorods, and nanoparticles under the conditions of 550 ppm of NO, 550 ppm of NH_3, 6% of O_2, 2.5% of H_2O (when added), and GHSV of 36,000 h^{-1}.

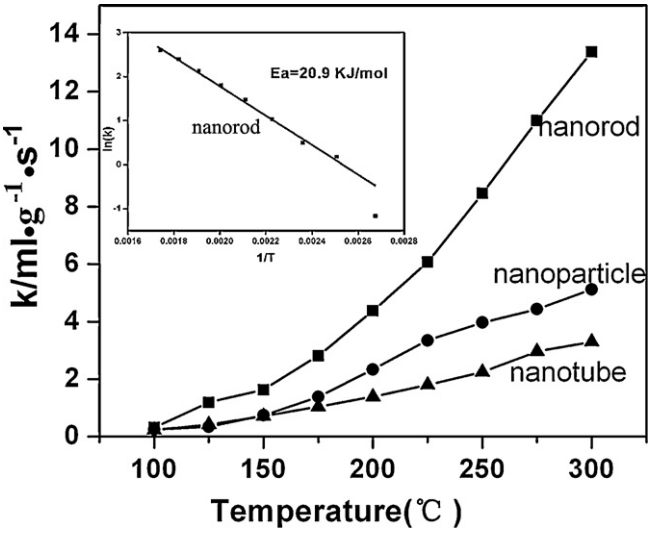

Fig. 7. Reaction rate coefficient of MnO_2 nanotubes, nanorods, and nanoparticles. The inset is Arrhenius plot of MnO_2 nanorods.

approximately 1:0.54:1.67 (mainly weak acid sites for nanotubes), respectively.

3.4. Catalytic activity characterization

Fig. 6 shows the NO_x conversion efficiency as a function of temperatures over different catalysts. For nanotubes, the efficiencies were all very low in the investigated temperature window, and the best efficiency of 60.8% was attained at 300 °C. The nanoparticles had efficiencies of below 80% in the temperature window, and the best efficiency of 78.5 at 300 °C. The nanorods present the highest activity for reduction of NO_x in the investigated temperature window from 100 to 300 °C with efficiency of above 90% between 250 and 300 °C and the highest removal efficiency of 98.2% at 300 °C. The NO_x conversion for the nanotubes and nanoparticles in the studied temperature range was always lower than that for nanorods. Moreover, the catalytic properties of all catalysts increased with temperature from 100 to 300 °C.

To better evaluate the catalytic activity, kinetic parameters were calculated according to the following equation from the NO_x conversion [32–34]:

$$k = -\frac{V}{W} \times \ln(1 - x). \quad (1)$$

In the above equation, k is the reaction rate coefficient ($ml\,g^{-1}\,s^{-1}$), V is the total gas flow rate ($ml\,s^{-1}$), W is the mass of catalysts in the reactor, and x is the conversion of NO_x in the testing activity. This equation is based on the theory that the reaction is first-order dependent on NO_x and zero-order dependent on NH_3 [35–37]. A high reaction constant of MnO_2 nanorods shown in Fig. 7 was observed clearly, especially in the high temperature range. The improvement in the catalytic rate of catalysts at high temperature is much greater than that at low temperatures. The rate constant for MnO_2 nanorods at 300 °C was 13.4 $ml\,g^{-1}\,s^{-1}$, which was much higher than that of the nanoparticles (5.12 $ml\,g^{-1}\,s^{-1}$) and nanotubes (3.30 $ml\,g^{-1}\,s^{-1}$). The apparent activation energy was calculated using the Arrhenius equation given by:

$$k = k_0 e^{-E_a/RT}. \quad (2)$$

In the above, E_a is the apparent activation energy. It can be calculated from the slope of the curve $\ln(k)$ versus $1/T$ as the inset in Fig. 7 shown, apparent activation energies of SCR reaction on the MnO_2 nanorods, nanotubes, and nanoparticles were 20.9, 21.0 and 36.6 kJ/mol, respectively. In view of kinetics, the surface of MnO_2 nanorods was favorable to SCR reaction. Furthermore, the reaction constant of nanorods was much higher than that of nanotubes and nanoparticles, so the SCR reaction occurred quickly there. From the apparent activation energy, less energy was needed for activation in the SCR reaction on the nanorods. Therefore, the MnO_2 nanorods had the best efficiency among the three catalysts.

Based on the analysis of XPS and TPR, the MnO_2 nanorods and nanoparticles showed more O_L groups and high reducibility, thereby contributing to the catalytic activity. However, total NH_3 desorbed from MnO_2 nanoparticles was only approximately half of those desorbed from the nanorods. Accordingly, MnO_2 nanorods had a large number of strong acid sites, which favored SCR reaction.

Given that water vapor is always included in the feed gas stream containing NO_x to be removed, Fig. 6 also shows the effect of water vapor on the NO_x removal over the MnO_2 nanorod catalyst after stabilization. When 2.5% H_2O was added, a slight decline in NO_x conversion (from 98% to 92% at 300 °C) was observed, indicating that the inhibition effect of H_2O on the SCR activity over MnO_2 nanorods was almost negligible. The inhibition effect could be ascribed to the competition adsorption between water and ammonia on acid sites [19].

The HRTEM (not showed here) showed that the MnO_2 nanotubes and nanorods grew along the c-axis, in agreement with results reported in literature [20,21]. For nanoparticles, the determination of its surface structure is difficult because of their poly-morphological structure. Although further study is needed to clarify the relationship between the atomic structure of catalyst surface and the corresponding catalytic activity, it seems that MnO_x nanorods showed excellent NH_3 adsorbability and high lattice oxygen concentration, which favored the de-NO_x reaction.

4. Conclusion

MnO_2 nanotubes, nanorods, and nanoparticles have been prepared using a hydrothermal method, after which the different SCR activities of NO_x were studied and compared. MnO_2 nanorods showed the best efficiency among the three different-shaped MnO_2 at low temperature (100–300 °C) under a GHSV of 36,000 h^{-1}. Based on the XRD, SEM, XPS, TPD and TPR analyses, the high efficiency of MnO_2 nanorods could be ascribed to low crystallinity, more lattice oxygen, high reducibility, and a large number of strong acid sites. The apparent activation energy of the SCR reaction on the surface

of nanorods has been calculated to be 20.9 kJ/mol, which is in favor of the reaction compared with the two other catalysts.

Acknowledgements

This work was supported by the United Nations Industrial Development Organization (UNIDO) (Project No. TF/CPR/03/006), Environmentally Sustainable Management of Medical Wastes in China (Contract No: C/V/S/10/251), the National Foundation of Zhejiang Province, China (Grant No. Z4080070), the Foundation of Science and Technology Bureau of Zhejiang Province, China (Grant Nos. 2008C21057 and 2009C34003), and the Fundamental Research Funds for the Central Universities (Program No. 2010QNA4005).

References

[1] G. Busca, L. Lietti, G. Ramis, F. Berti, Chemical and mechanistic aspects of the selective catalytic reduction of NO_x by ammonia over oxide catalysts: a review, Appl. Catal. B: Environ. 18 (1998) 1–36.
[2] H. Hamada, Selective reduction of NO by hydrocarbons and oxygenated hydrocarbons over metal-oxide catalysts, Catal. Today 22 (1994) 21–40.
[3] V.I. Parvulescu, P. Grange, B. Delmon, Catalytic removal of NO, Catal. Today 46 (1998) 233–234.
[4] J.N. Armor, Environmental catalysis, Appl. Catal. B: Environ. 1 (1992) 221–256.
[5] W.S. Kijlstra, J.C.M.L. Daamen, J.M. van de Graff, B.V. Linden, E.K. Poels, A. Bliek, Inhibiting and deactivating effects of water on the selective catalytic reduction of nitric oxide with ammonia over MnO_x/Al_2O_3, Appl. Catal. B: Environ. 7 (1996) 337–357.
[6] H. Bosch, F.J.I.G. Janssen, Catalytic reduction of nitrogen oxides, Catal. Today 2 (1988) 369–379.
[7] H.H. Phil, M.P. Reddy, P.A. Kumar, L.K. Ju, J.S. Hyo, SO_2 resistant antimony promoted V_2O_5/TiO_2 catalyst for NH_3-SCR of NO_x at low temperatures, Appl. Catal. B: Environ. 78 (2008) 301–308.
[8] J. Muniz, G. Marban, A.B. Fuertes, Low temperature selective catalytic reduction of NO over modified activated carbon fibres, Appl. Catal. B: Environ. 27 (2000) 27–36.
[9] A.K.H. Nohman, D. Duprez, C. Kappenstein, S.A.A. Mansour, M.I. Zaki, in: B. Delmon, P.A. Jacobs, G. Poncelet (Eds.), Preparation of Catalyst, V, Elsevier, Amsterdam, 1991, p. 617.
[10] R. Craciun, B. Nentwick, K. Hadjiivanov, H. Knozinger, Structure and redox properties of MnO_x/yttrium-stabilized zirconia (YSZ) catalyst and its used in CO and CH_4 oxidation, Appl. Catal. A: Gen. 243 (2003) 67–79.
[11] R. Craciun, N. Dulamita, Ethylbenzene oxidative dehydrogenation on MnO_x/SiO_2 catalysts, Ind. Eng. Chem. Res. 38 (1999) 1357–1363.
[12] T. Yamashita, A. Vannice, NO decomposition over Mn_2O_3 and Mn_3O_4, J. Catal. 163 (1996) 158–168.
[13] C. Lahousse, A. Bernier, P. Grange, B. Delmon, P. Papaefthimiou, T. Ioannides, X. Verykiosy, Evaluation of gamma-MnO_2 as a VOC removal catalyst: comparison with a noble metal catalyst, J. Catal. 178 (1998) 214–225.
[14] C. Reed, Y. Xi, S.T. Oyama, Distinguishing between reaction intermediates and spectators: a kinetic study of acetone oxidation using ozone on a silica-supported manganese oxide catalyst, J. Catal. 235 (2005) 378–392.
[15] L. Singoredjo, R. Korver, F. Kapteijn, J. Moulijn, Alumina supported manganese oxides for the low-temperature selective catalytic reduction of nitric-oxide with ammonia, Appl. Catal. B: Environ. 1 (1992) 297–316.
[16] U. Bentrup, A. Bruckner, M. Richter, R. Fricke, NO_x adsorption on MnO_2/NaY composite: an in situ FTIR and EPR study, Appl. Catal. B: Environ. 32 (2001) 229–241.
[17] G.S. Qi, R.T. Yang, R. Chang, Low-temperature SCR of NO with NH_3 over USY-supported manganese oxide-based catalysts, Catal. Lett. 87 (2003) 67–71.
[18] Li J.H., J.J. Chen, R. Ke, C.K. Luo, J.M. Hao, Effects of precursors on the surface Mn species and the activities for NO reduction over MnO_x/TiO_2 catalysts, Catal. Commun. 8 (2007) 1896–1900.
[19] X.L. Tang, J.M. Hao, W.G. Xu, J.H. Li, Low temperature selective catalytic reduction of NO_x with NH_3 over amorphous MnO_x catalysts prepared by three methods, Catal. Commun. 8 (2007) 329–334.
[20] J. Luo, H.T. Zhu, H.M. Fan, J.K. Liang, H.L. Shi, G.H. Rao, J.B. Li, Z.M. Du, Z.X. Shen, Synthesis of single-crystal tetragonal α-MnO_2 nanotubes, J. Phys. Chem. C 112 (2008) 12594–12598.
[21] J.T. Sampanthar, J. Dou, G.G. Joo, E. Widjaja, L.Q.H. Eunice, Template-free low temperature hydrothermal synthesis and characterization of rod-shaped manganese oxyhydroxides and manganese oxides, Nanotechnology 18 (2007) 025601–025609.
[22] J.T. Sampanthar, J. Dou, G.Ge. Joo, E. Widjaja, L.Q.H. Eunice, Template-free low temperature hydrothermal synthesis and characterization of rod-shaped manganese oxyhydroxides and manganese oxides, Nanotechnology 18 (2007) 025601–025609.
[23] E. Lopez-Navarrete, A. Caballero, A.R. Gonzalez-Elipe, M. Ocana, Chemical state and distribution of Mn ions in Mn-doped alpha-Al_2O_3 solid solutions prepared in the absence and the presence of fluxes, J. Eur. Ceram. Soc. 24 (2004) 3057–3062.
[24] G. Carja, Y. Kameshima, K. Okada, C.D. Madhusoodana, Mn–Ce/ZSM5 as a new superior catalyst for NO reduction with NH_3, Appl. Catal. B: Environ. 73 (2007) 60–64.
[25] C.L. Qin, J.J. Oak, N. Ohtsu, K. Asami, A. Inoue, XPS study on the surface films of a newly designed Ni-free Ti-based bulk metallic glass, Acta Mater. 55 (2007) 2057–2063.
[26] X.F. Tang, J.H. Li, L. Sun, J.M. Hao, Origination of N_2O from NO reduction by NH_3 over β-MnO_2 and α-Mn_2O_3, Appl. Catal. B: Environ. 99 (2010) 156–162.
[27] F. Arena, T. Torre, C. Raimondo, A. Parmaliana, Structure and redox properties of bulk and supported manganese oxide catalysts, Phys. Chem. Chem. Phys. 3 (2001) 1911–1917.
[28] F. Kapteijn, L. Singoredjo, A. Andreini, J.A. Moulijn, Activity And Selectivity of pure manganese oxides in the selective catalytic reduction of nitric-oxide with ammonia, Appl. Catal. B: Environ. 3 (1994) 173–189.
[29] J. Carno, M. Ferrandon, E. Bjornbom, S. Jaras, Mixed manganese oxide platinum catalysts for total oxidation of model gas from wood boilers, Appl. Catal. A: Gen. 155 (1997) 265–281.
[30] M. Mhamdi, S. Khaddar-Zine, A. Ghorbel, Influence of the cobalt salt precursors on the cobalt speciation and catalytic properties of H-ZSM-5 modified with cobalt by solid-state ion exchange reaction, Appl. Catal. A: Gen. 357 (2009) 42–50.
[31] L. Chmielarz, P. Kustrowski, M. Zbroja, B. Gil-Knap, J. Datka, R. Dziembaj, SCR of NO by NH_3 on alumina or titania pillared montmorillonite modified with Cu or Co: Part II. Temperature programmed studies, Appl. Catal. B: Environ. 53 (2004) 47–61.
[32] D.M. Amiridis, V.D. Robert, E.W. Israel, The effect of metal oxide additives on the activity of V_2O_5/TiO_2 catalysts for the selective catalytic reduction of nitric oxide by ammonia, Appl. Catal. B: Environ. 20 (1999) 111–122.
[33] M. Casapu, O. Krocher, M. Elsener, Screening of doped MnO_x–CeO_2 catalysts for low-temperature NO-SCR, Appl. Catal. B: Environ. 88 (2009) 413–419.
[34] X.Y. Guo, C. Bartholomew, W. Hecker, L.L. Baxter, Effects of sulfate species on V_2O_5/TiO_2 SCR catalysts in coal and biomass-fired systems, Appl. Catal. B: Environ. 92 (2009) 30–40.
[35] T. Komatsu, M. Nunokawa, I.S. Moon, T. Takahara, S. Namba, T. Yashima, Kinetic studies of reduction of nitric oxide with ammonia on Cu^{2+}-exchanged zeolites, J. Catal. 148 (1994) 427–437.
[36] E.Y. Choi, I.S. Nam, Y.G. Kim, TPD study of mordenite-type zeolites for selective catalytic reduction of NO by NH_3, J. Catal. 161 (1996) 597–604.
[37] R.Q. Long, R.T. Yang, FTIR and kinetic studies of the mechanism of Fe^{3+}-exchanged TiO_2-pillared clay catalyst for selective catalytic reduction of NO with ammonia, J. Catal. 190 (2000) 22–31.